Advanced Controller of a Hybrid Foil-magnetic Bearing

Ye Tian[a], Yanhua Sun[b], Lie Yu[c]

State Key Laboratory for Strength and Vibration of Mechanical Structures, Xi'an Jiaotong University, No.28 Xianning West Road, Xi'an, 710049, Shaanxi Province, China,
[a]a.g.o.u2@stu.xjtu.edu.cn
[b]sunyanhua@mail.xjtu.edu.cn
[c]yulie@mail.xjtu.edn.cn

Abstract—A hybrid foil-magnetic bearing (HFMB) is combination of a gas foil bearing (GFB) and a active magnetic bearing (AMB), which takes advantages of both bearings while compensating each other's weaknesses. It is a solution of friction and wear of the GFBs at low speeds and limited load capacity of the AMBs. Furthermore, load sharing and control of dynamics can be achieved in a hybrid foil-magnetic bearing. However, in order to achieve the ideal performances of the HFMBs, an advanced controller must be designed based on the static and dynamic performances of the HFMBs. Since the AMBs are 'smart' devices that the working condition can be measured and actively controlled, it is quite natural to design an advanced controller for the HFMBs to use the AMBs to identify the characteristics of the GFBs and with the function of load sharing between the GFBs and the AMBs. In this paper, a 4-DOF model of bearing-rotor system supported by two HFMBs was established firstly, and then an advanced controller with the function of identification and load sharing was presented. Finally, experiments were done on a test rig whose rotor is supported by two journal HFMBs and a thrust AMB. The test results show that when change the load shared by the GFBs and the AMBs, advanced controller can find the new proper working position of the HFMBs rapidly and smoothly. More importantly, HFMBs with advanced controller based on the identified characteristics of GFBs can work steadily at the speed range of 0~2,2000r/min.

I. INTRODUCTION

AMBs and GFBs are two typical bearings for the high speed rotating machines. Each bearing has its own advantages and disadvantages. The AMB generates magnetic force to support rotors without contact. There is no need of lubrication or sealing, and the wear is completely eliminated. Furthermore the working condition of AMBs can also be measured and actively controlled. However, because of magnetic saturation and thermal effect, the load capacity of AMBs is limited [1-2]. The GFB provides another non-contact way to support the high speed rotor. GFB is self-acting hydrodynamic bearing that uses ambient air or any process gas as the lubricating fluid. A hydrodynamic film pressure builds up within the small gap between the rotating shaft and the smooth foil. It has simple structure and favorable adaptability, and can work in high temperature circumstance. Its weakness is the contact and friction between the bearing and the journal at low speeds, which reduce the life of GFBs greatly. Moreover, it also has low load capacity at low speeds [3-7]. A HFMB is a combination of a GFB and an AMB and can share the load between them. The HFMB has the advantages of both bearings. It can improve not only the load carrying capacity but also the dynamic performance of the rotor-bearing system [8-11]. The HFMB is an ideal manner of the high speed rotating machines.

The control system is very important in operation of a HFMB. Using a conventional PID control algorithm, the controller would attempt to force the journal to a referred position at all times regardless of loads. However, in a loaded foil bearing, the journal runs at some eccentricity and attitude angle when supporting a load. Heshmat, Chen, and Walton did a great job in solving the contradiction, they used a supervisory control system to ensure the functionality of the hybrid bearings [9,10,12]. However, the supervisory control system strongly depends on the characteristics of GFBs obtained from numerical calculation or independent bearing experiments. If different GFBs are used or the working conditions are changed, numerical calculation or independent bearing experiments must be done again, and the control system should be adjusted as well. It causes repetitive work and takes a long time. Since the AMBs are 'smart' devices that the working condition can be measured and actively controlled, it is quite natural to design an advanced controller for HFMBs to use AMBs identify the characteristics of GFBsand with the function of load sharing between GFBs and AMBs[13, 14].

In this paper, a 4-DOF model of bearing-rotor system supported by two journal HFMBs was established firstly. Then an advanced controller with was presented. Dynamic loads were applied by two radial AMBs, and a frequency domain identification method was presented to identify the stiffness and damping coefficients of the GFBs. After that, a searching algorithm was presented to determine the static working position of the HFMBs with different sharing load. The test results show the advanced controller can rapidly find the new working position of HFMBs by using a searching algorithm when the load shared by GFBs and AMBs are changed. Furthermore, HFMBs with advanced controller work steadily in the transient operation tests.

A. *Hybrid Foil-magnetic Bearings*

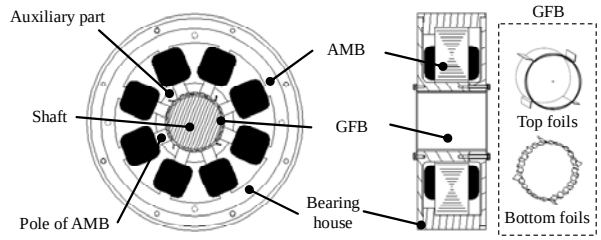

Figure 1. Structure of the HFMB

The structure of the HFMB studied in this paper is shown in Fig.1. The GFB consists of four top foil each supported by a bottom bump foils. All these foils are located in the air gap between the AMB poles and the journal of the rotor. The foils are made of non-magnetic materials so that they will not affect work of the AMB. The applied forces on the shaft generated by the AMB can be calculated using the following formula [15]:

$$f_n = ek_{th}\left(\frac{i_1^2}{G_1^2}-\frac{i_2^2}{G_2^2}\right),\ (n=x,y) \tag{1}$$

where k_{th} is a constant related to the AMB, i_1 and i_2 are the currents in the opposing coils, G_1 and G_2 are the upper and lower air gaps, and e is a derating factor. A series calibrations were conducted by applying deadweight to the AMB in multiple orientations beforehand witch makes the mean error of static forces within 2%.

B. *Dynamic Model of 4-DOF Bearing-rotor System*

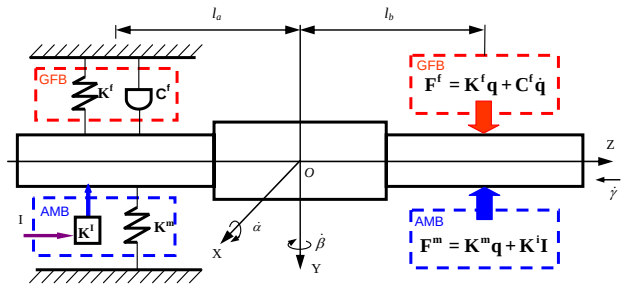

Figure 2. Schematic of the dynamic model

When the ratio of the rotor length to the diameter of the thrust disc is relatively large, influences of the thrust bearing to radial motion of the rotor can be neglected [2]. Therefore, the axial motion of the rotor could be studied separately. A rigid rotor supported by two radial bearings is shown in Fig.2. The distant between bearing locations is l and O is the mass center of the rotor. Define the journal displacements at the left journal bearing as x_a and y_a, and the displacements at the right journal bearing as x_b and y_b. The distant between mass center to the left and right HFMBs are l_a and l_b respectively. The rotation angle in the XZ plane is $\alpha=(x_b - x_a)/l$ and the rotation angle in the Y-Z plane is $\beta=(y_b - y_a)/l$. Both the GFB and the AMB at the left side are the same as the right ones; hence the stiffness and damping coefficients at left side and right side use the same expressions.

The generalized displacements are defined as $\mathbf{q}_m = [x, y, \alpha, \beta]^T$, where x and y are the displacements of its center of mass O The radial displacements of the journal at bearing positions are defined as: $\mathbf{q} = [x_a, x_b, y_a, y_b]^T$. The equations of motion of the rotor are:

$$\begin{cases} (1-a)\,m\,\ddot{x} + \Delta F_{xa} + \Delta F_{xb} = f_x \\ a\,m\,\ddot{y} + \Delta F_{ya} + \Delta F_{yb} = f_y \\ J_y\ddot{\beta} + \dot{\gamma} J_z \dot{\alpha} = a\,l\,\Delta F_{xa} - (1-a)\,l\,\Delta F_{xb} \\ J_x\ddot{\alpha} - \dot{\gamma} J_z \dot{\beta} = a\,l\,\Delta F_{ya} - (1-a)\,l\,\Delta F_{yb} \end{cases} \tag{2}$$

where, m is the mass of the rotor, $\dot{\gamma}$ is the rotational speed, f_x and f_y are the external forces, J_x, J_y and J_z are moment of inertia of rotor at rotary point O. $\Delta F_{xa}, \Delta F_{xb}, \Delta F_{ya}$ and ΔF_{yb} are bearing forces in the X and Y directions.

$$\begin{cases} \Delta F_{xa} = k_x^m x_a + k_x^i i_{xa} + k_{xx}^f x_a + k_{yx}^f y_a + c_{xx}^f \dot{x}_a + c_{yx}^f \dot{y}_a \\ \Delta F_{xb} = k_x^m x_b + k_x^i i_{xb} + k_{xx}^f x_b + k_{yx}^f y_b + c_{xx}^f \dot{x}_b + c_{yx}^f \dot{y}_b \\ \Delta F_{ya} = k_y^m y_a + k_y^i i_{ya} + k_{yy}^f y_a + k_{xy}^f x_a + c_{yy}^f \dot{y}_a + c_{xy}^f \dot{x}_a \\ \Delta F_{yb} = k_y^m y_b + k_y^i i_{yb} + k_{yy}^f y_b + k_{xy}^f x_b + c_{yy}^f \dot{y}_b + c_{xy}^f \dot{x}_b \end{cases} \tag{3}$$

where i_{xa}, i_{xb}, i_{ya} and i_{ya} are the control currents. k_x^m, k_y^m are the force/displacement stiffness and k_x^i, k_y^i are force/current stiffness of the AMB. $k_{xx}^f, k_{xy}^f, k_{yx}^f, k_{yy}^f$ are the stiffness coefficients and $c_{xx}^f, c_{xy}^f, c_{yx}^f, c_{yy}^f$ are the damping coefficients of GFB. The equations of motion can also be written as:

$$\mathbf{M}\ddot{\mathbf{q}} + \mathbf{C}^f\dot{\mathbf{q}} + (\mathbf{K}^f - \mathbf{K}^m)\mathbf{q} = \mathbf{K}^i\mathbf{I} \tag{4}$$

$$\mathbf{M} = \begin{bmatrix} (1-a)m & am & 0 & 0 \\ 0 & 0 & (1-a)m & am \\ -J_y/l & J_y/l & 0 & 0 \\ 0 & 0 & -J_x/l & J_x/l \end{bmatrix},$$

$$\mathbf{C}^f = \begin{bmatrix} c_{xx}^f & c_{xx}^f & c_{xy}^f & c_{xy}^f \\ c_{yx}^f & c_{yx}^f & c_{yy}^f & c_{yy}^f \\ -alc_{xx}^f & (1-a)lc_{xx}^f & -alc_{xy}^f - \dot{\gamma}J_z/l & (1-a)lc_{xy}^f + \dot{\gamma}J_z/l \\ -alc_{yx}^f + \dot{\gamma}J_z/l & (1-a)c_{yx}^f - \dot{\gamma}J_z/l & -alc_{yy}^f & (1-a)lc_{yy}^f \end{bmatrix},$$

$$\mathbf{K}^f = \begin{bmatrix} k_{xx}^f & k_{xx}^f & k_{xy}^f & k_{xy}^f \\ k_{yx}^f & k_{yx}^f & k_{yy}^f & k_{yy}^f \\ -alk_{xx}^f & (1-a)lk_{xx}^f & -alk_{xy}^f & (1-a)lk_{xy}^f \\ -alk_{yx}^f & (1-a)k_{yx}^f & -alk_{yy}^f & (1-a)lk_{yy}^f \end{bmatrix}, \tag{5}$$

$$\mathbf{K}^m = \begin{bmatrix} k_x^m & k_x^m & 0 & 0 \\ 0 & 0 & k_y^m & k_y^m \\ -alk_x^m & (1-a)lk_x^m & 0 & 0 \\ 0 & 0 & -alk_y^m & (1-a)lk_y^m \end{bmatrix},$$

$$\mathbf{K}^i = \begin{bmatrix} k_x^i & k_x^i & 0 & 0 \\ 0 & 0 & k_y^i & k_y^i \\ -alk_x^i & (1-a)lk_x^i & 0 & 0 \\ 0 & 0 & -alk_y^i & (1-a)lk_y^i \end{bmatrix}, \mathbf{I} = \begin{bmatrix} i_{xa} \\ i_{xb} \\ i_{ya} \\ i_{yb} \end{bmatrix}$$

$\mathbf{M}$ is the mass matrix, $\mathbf{K}^m$ and $\mathbf{K}^i$ are the force/displacement matrix and force/current matrix of the AMB, $\mathbf{K}^f$ and $\mathbf{C}^f$ are the stiffness and the damping matrices of the GFB, $\mathbf{I}$ is the control currents vector. The elements of matrix $\mathbf{K}^m$ and $\mathbf{K}^i$ can be obtained by linearizing Eq. (1) for small rotor

displacements around the operating point. Take X direction for instance, linearized AMB force around operating point (x_0, i_{x0}) can be written as

$$f_x^m = \frac{\partial f_x}{\partial x}|_{x=x_0}\ x + \frac{\partial f_x}{\partial i}|_{i=i_{x0}}\ i_x = k_x^m x + k_x^i i_x \qquad (6)$$

The matrices $\mathbf{K^m}$ and $\mathbf{K^i}$ of the GFB are unknown which need to be identified.

C. Advanced Control System

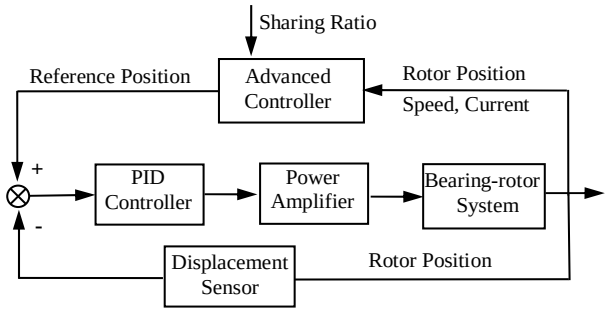

Figure 3. Schematic control system

The control system is designed as shown in Fig.3. It consists of a transient feedback control loop of the AMBs and an advanced controller which has the function of identification and load sharing. In the transient control loop, decoupling control is employed. At each DOF, a PID controller is used to ensure the shaft working at the reference position determined by the advanced controller. For identification of the characteristics of GFBs, the advanced controller output harmonic signals which lead to harmonic excitation of magnetic forces. With the function of sharing load between the GFBs and the AMBs, the advanced controller output constant signals based on the load sharing ratio λ, rotating speed ω, control current I and shaft position q.

Identify the dynamic characteristics of GFBs

For the harmonic excitation with an arbitrary excitation frequency ω, Eq. (4) can be rewritten as

$$\begin{bmatrix} D_{11} & D_{12} & D_{13} & D_{14} \\ D_{21} & D_{22} & D_{23} & D_{24} \\ D_{31} & D_{32} & D_{33} & D_{34} \\ D_{41} & D_{42} & D_{43} & D_{44} \end{bmatrix} \begin{Bmatrix} x_a(\omega) \\ x_b(\omega) \\ y_a(\omega) \\ y_b(\omega) \end{Bmatrix} = \begin{Bmatrix} i_{xa}(\omega) \\ i_{xb}(\omega) \\ i_{ya}(\omega) \\ i_{yb}(\omega) \end{Bmatrix} \qquad (7)$$

where

$$\begin{aligned}
&D_{11} = \left\{k_{xx}^f - k_x^m - \omega^2\left[J_y / l^2 + (1-a)^2 m\right] + j\omega c_{xx}^f\right\} / k_x^i, D_{14} = 0 \\
&D_{12} = \omega^2\left[J_y / l^2 - (1-a)am\right] / k_x^i, D_{13} = \left(k_{xy}^f + j\omega c_{xy}^f\right) / k_x^i; \\
&D_{21} = \omega^2\left[J_y / l^2 - (1-a)am\right] / k_x^i, D_{24} = \left(k_{xy}^f + j\omega c_{xy}^f\right) / k_x^i, \\
&D_{22} = \left[k_{xx}^f - k_x^m - \omega^2\left(J_y / l^2 + a^2 m\right) + j\omega c_{xx}^f\right] / k_x^i, D_{23} = 0; \\
&D_{31} = \left(k_{yx}^f + j\omega c_{yx}^f\right) / k_x^i, D_{34} = \omega^2\left[J_x / l^2 - (1-a)am\right] / k_x^i, \\
&D_{33} = \left\{k_{yy}^f - k_y^m - \omega^2\left[J_x / l^2 + (1-a)^2 m\right] + j\omega c_{yy}^f\right\} / k_x^i, D_{32} = 0; \\
&D_{41} = 0, D_{44} = \left[k_{yy}^f - k_y^m - \omega^2\left(J_x / l^2 + a^2 m\right) + j\omega c_{yy}^f\right] / k_x^i, \\
&D_{43} = \omega^2\left[J_x / l^2 - (1-a)am\right] / k_x^i, D_{42} = \left(k_{yx}^f + j\omega c_{yx}^f\right) / k_x^i,
\end{aligned} \qquad (8)$$

The dynamic coefficients of the GFB can be obtained experimentally by separating the real and imaginary part from the measured dynamic stiffness D_{mn} (m, n =1, 2, 3, 4). See ref. [14] for more details of identification of the GFBs parameters by using the AMBs as exciters.

Load sharing between the GFB and the AMB

The total bearing force F^B of the HFMB includes two parts, the force of the GFB F^f and the force of the AMB F^m. Define the load sharing ratio of F^f to F^B as λ. The total bearing force F^B equals to the rotor gravity.

$$F^B = F^m + F^f = G = \lambda G + (1-\lambda)G \qquad (9)$$

Since both the forces of the GFB and the AMB are functions of the working place q [2,6], sharing the load between the GFB and the AMB can be achieved by finding a proper working position where the forces satisfy the following condition, where e_0 is the coefficient of precision.

$$\frac{\left|F^f(q_B) - (1-\lambda)G\right|}{\left|(1-\lambda)G\right|} \le e_0 \text{ or } \frac{\left|F^m(q_B) - \lambda G\right|}{\left|\lambda G\right|} \le e_0 \qquad (10)$$

Use equilateral triangles to divide the working plane of the HFMB. And the working position can be obtained through continuous searching and dividing of the journal working area. Fig.4 (a) shows the initial working areas of the GFB, the AMB and the HFMB. Fig.4 (b) shows the initial area Δ123. The vertexes of Δ123 are the midpoints of the sides of the inscribed triangle of the bearing boundary circle.

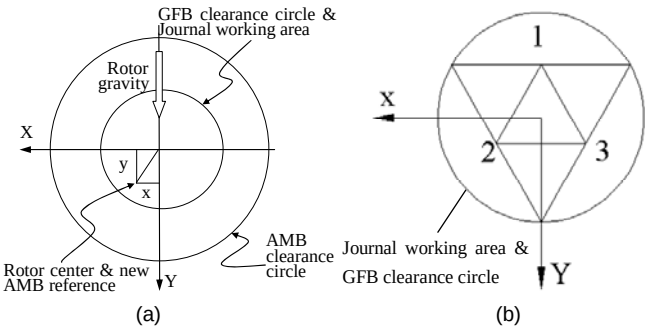

Fig. 4 Journal working area and initial Area

Define the vectors of AMB forces at vertices as $F^m(k) = [F_x^m(k), F_y^m(k)]^T$, k=1,2,3. The predetermined sharing load of the AMB are $F_s^m(k) = [F_{xs}^m(k), F_{ys}^m(k)]^T$, the difference vectors are $F_e^m(k) = F^m - F_s^m = [F_{xe}^m(k), F_{ye}^m(k)]^T$. So the total differences of forces are $F_e(k) = |F_e^m(k)|$, k=1,2,3. The steps of searching the working position are as follows

Step1. Move the journal center to the vertices of the initial triangle area calculate the forces of AMB and store.

Step2. Decide the next triangle area to be moved in based on the stored data. If the next area is in the present area, go to step 4, else go to step 3.

Step3. Move the journal center to the vertices of the next triangle area calculate the forces of AMB and store.

Step4. Divide the present area; the vertexes of the next triangle area are the midpoints of the sides of the present one. End searching if Eq. (10) is satisfied, else go to step 3.

The next triangle area can be decided as follows.

Define the vector of symbol coefficients $coe(k)=[coe_x(k),coe_y(k)]^{\mathrm{T}}$ for every side of Δ123

$$\text{if}\begin{cases}F_{ie}^{m}(k)\times F_{ie}^{m}(k+1)>0,(k=1,2)\\ F_{ie}^{m}(k)\times F_{ie}^{m}(k-2)>0,(k=3)\end{cases},(i=x,y)$$

then $coe_i(k)=1$, else $coe_i(k)=0$

Thus the four possible conditions of *coe*(*k*) at each side of Δ123 are shown in Fig.5. (Permutation of vertices 1,2,3 do not affect the determination, and "01" equals to "10").

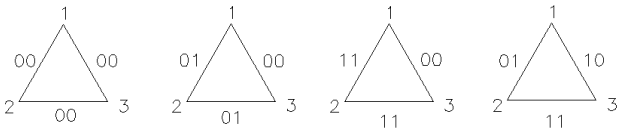

(a) (b) (c) (d)

Fig. 5 Possible conditions of *coe*(*k*)

Case (a): Plus $F_e(k)$ of every side of Δ123 and find the minimum: min($F_e(1)+F_e(2)$, $F_e(2)+F_e(3)$, $F_e(3)+F_e(1)$).The side with the minimum value is the common side of the next triangle area and the present triangle area.

Case (b): Plus $F_e(k)$ of the side of Δ123 where the symbol coefficient is 01 and find the minimum. Take Fig.10 (b) for example, find min($F_e(1)+F_e(2)$, $F_e(2)+F_e(3)$). The side with the minimum value is the common side of the next triangle area and the present triangle area.

Case (c) or (d): The vertexes of the next triangle area are the midpoints of the sides of the present one.

D. Experiments

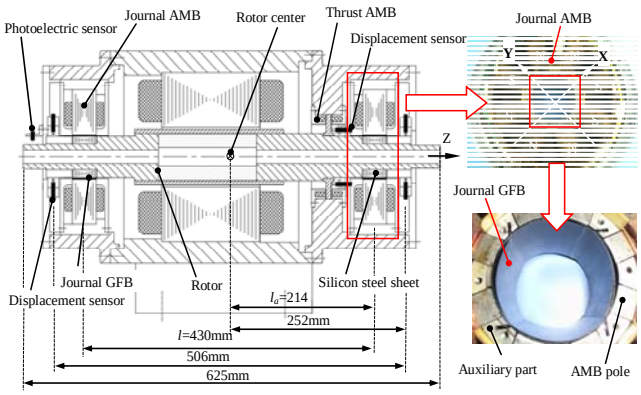

Figure 6. Schematic diagram of the test rig

Figure 6 displays the schematic diagram of the test rig and the photograph of the journal HFMB. There are ten eddy current displacement sensors, eight of them fixed beside the journal bearings measuring the displacements in X and Y direction in differential manner and the rest two fixed beside the thrust bearing measuring the axial displacements. A photoelectric sensor is used to measure the rotating speed, and the currents of the AMB coils are measured by current sensors which are not shown in Fig. 6. All these sensor signals are saved into a PC equipped with a commercial I/O boards. Parameters of the HFMB, the rotor and the control system are shown in Table 1. The parameters of PID controller are determined using a LQG method mentioned in reference [16].

TABLE I. PARAMETERS OF THE HFMB, THE ROTOR AND THE CONTROL SYSTEM

Parameters and dimensions	Values
Bearing housing inner diameter, D_h	61.4 mm
Axial bearing length, L	60 mm
Rotor diameter, d	59.8 mm
Arc length of the top foil, L_t	90 mm
Arc length of the bump foil, L_b	46.5 mm
Number of the bumps per bump foil, *num*	16
Top foil thickness, t_t	0.18 mm
Bump foil thickness, t_b	0.1 mm
Nominal clearance, C	0.14mm
Bump pitch, s_0	3.1 mm
Bump length, l_0	1.8 mm
Bump height, h_b	0.3 mm
Poisson's ratio, v	0.29
Modulus of elasticity, E	213.73 MPa
Ambient pressure, P_a	103.4 kPa
Lubricant viscosity, μ	2.896×10^{-5} Pa·s
Rotor mass, m	15.5 kg
Bias current of AMB, I_0	4 A
Number of turns of the coil windings, N	97
Air permeability, μ_0	$4\pi\times10^{-7}$N/A^2
Projection area of the magnetic pole, A	4.54×10^{-4}m^2
Gain of the power amplifier, A_a	50 A/V
Decay time of the power amplifier, T_a	3×10^{-5} s
Gain of the displacement sensor, A_s	10V/m
Decay time of the displacement sensor, T_s	3×10^{-5} s
Proportional coefficient of the PID controller, K_{pr}	15
Integral coefficient of the the PID controller, K_{ir}	300 s^{-1}
Differential coefficient of the PID controller, K_{dr}	0.03
Differential time constant of PID controller, T_{dr}	0.009 s
Position precision coefficient, e_0	0.01

Load sharing tests

Load sharing tests were conducted under conditions of no shaft rotation. Set the value of load sharing ratio λ to 0, 0.5, and 1. The track of the journal canter and the difference value F_{ex}^{m}, F_{ey}^{m} are shown in Fig.7, Fig.8 and Fig.9 respectively. Results shown here are correspond to the right journal HFMB. Similar results are found for the left ones.

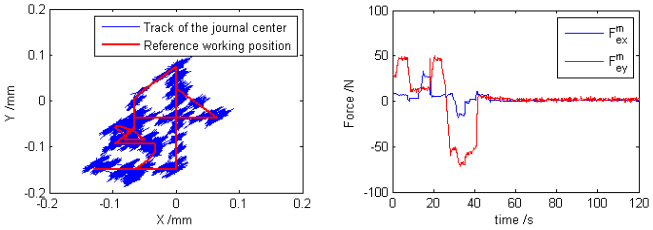

Figure 7. Schematic control system

In the case of λ=0 in Fig. 7, the GFBs take all the rotor gravity. The final position of the journal is (0.10mm,

0.09mm)^T. The difference value between AMB forces and sharing load F_{ex}^m=-1.5N, F_{ey}^m=0.5N.

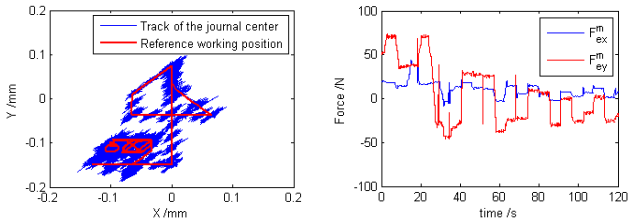

Figure 8. Schematic control system

In the case of λ=0.5 in Fig. 8, the AMBs take half of the rotor gravity. It shows that the final position of the journal is (0.08mm, 0.07mm)^T. The difference value between AMB forces and sharing load are F_{ex}^m=0.8N, F_{ey}^m=-0.2N.

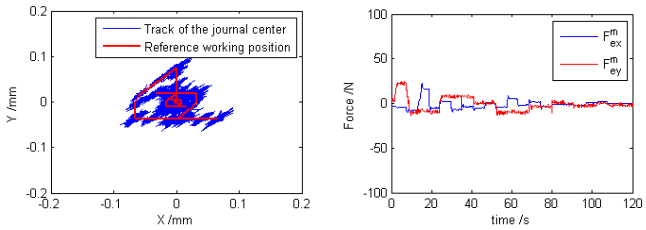

Figure 9. Schematic control system

In the case of λ=1 in Fig. 9, the AMBs take all of the rotor gravity. It shows that the final position of the journal is (0.01mm,-0.01mm)^T and the difference value between AMB forces and sharing load F_{ex}^m=-0.3N, F_{ey}^m=2.2N.

The results of load sharing tests show that the searching algorithm is able to locate the working position of the HFMB within a short time in different situations. Please note that the searching process only needs to be operated once before the uses of the HFMB and the position data are stored for future use.

Transient operation tests

Tests are conducted on the test rig to demonstrate the ability of the HFMB to support the rotor during transient events. The rotor was levitated by AMBs at zero speed and started to run up in the HFMB mode in order to evaluate the operation at increasing speeds, when the speed was above the GFB lift-off speed, the AMBs were tuned off to let rotor drop down on the GFBs in the GFB mode alone and the operation was evaluated. Finally the shaft was drove to slow down by the motor. Tests were successfully conducted at speeds up to 22,000rpm where AMB failures were simulated. Fig. 10 shows results of the shaft speed and the torque of the motor. The forces of the AMB and the rotor orbit are shown in Fig. 11 and Fig. 12 respectively.

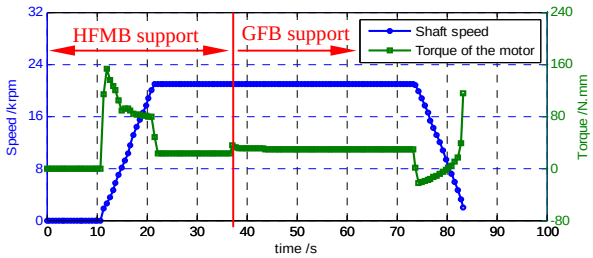

Figure 10. Shaft speed and motor torque vs. time

As shown in Fig. 10 there are peak signals of the motor torque caused by the friction between the shaft and GFBs during run-up and coast-down (Note that the negative value of the torque stands for the negative work generated by the motor when decelerate the shaft). When the speed was above the GFB lift-off speed, the torque quickly turns to a low value, a peak signal was caused by switching off the AMBs.

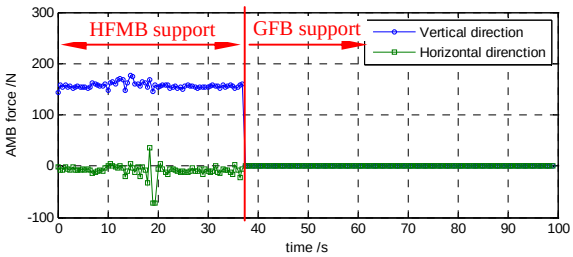

Figure 11. AMB forces vs. time

As shown in Fig. 11, since the rotor was levitated by AMBs at the center of the bearing housing at the beginning, the vertical force of AMBs equals to the gravity of rotor, the horizontal force of AMBs is almost zero. At the time when the AMBs were switched off, both the vertical and the horizontal forces of AMBs turn to zero.

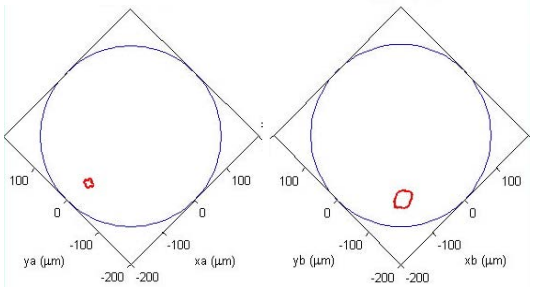

Figure 12. Shaft orbit at 22, 000rpm (supported by GFBs)

As shown in Fig. 12, the rotor orbit is stable at 22, 000rpm when the rotor is supported solely by the GFBs. Moreover, the final position of the journal is (-0.1mm, -0.1mm)^T, which is similar as the results shown in Fig. 7 with no shaft rotation. That means the working position of GFB is determined by structure deformation more than the gas films. Therefore, the results of load sharing tests of HFMBs under conditions of no shaft rotation can be used in a rotating bearing-rotor system.

E. Conclutions

An advanced controller of the HFMB is designed based on the 4-DOF bearing-rotor system in this paper. The characteristics of the GFB are identified using the AMBs as exciters and a frequency domain identification method was

presented to identify the stiffness and damping coefficients. A searching algorithm is proposed to locate the working position of the HFMB. The test results show that when change the load shared by the GFBs and the AMBs, advanced controller can find the new proper working position of HFMBs rapidly and smoothly. More importantly, HFMBs with advanced controller can work steadily at the speed range of 0~2,2000r/min.

REFERENCES

[1] Schweitzer G, Traxler A, and Bleuler H, 1993, "Mageticlager," Springer-Verlag Press, Berlin, pp. 14-16, 48-50, 197-202.

[2] Schweitzer, G., and Maslen, E. H., 2009, "Magnetic bearings: theory, design, and application to rotating machinery," Springer, Verlag Berlin Heidelberg, pp. 167-174.

[3] Wang Yunfei, 1999, "Gas Lubrication Theory and Gas Bearings Design," Beijing Mechanical Industry Press, Beijing, pp. 1-143.

[4] Ehrich F F, Jacobson S A, 2003, "Development of high-speed gas bearings for high-power density microdevices," *Journal of Engineering for Gas Turbines and Power*, 125(1), pp. 141-148.

[5] S. Jahanmir, H. Heshmat, and C. Heshmat, 2009, "Evaluation of DLC coatings for high-temperature foil bearing applications," *Journal of Tribology*, 131, pp. 011301.

[6] Geng Haipeng, Qi Shemiao,. YU Lie. "Analysis of the multileaf foil journal bearings with large preload effect," *Journal of Aerospace Power*, 2006, 21(3), pp. 569-574

[7] Liu L X, Teo C J, Epstein A H, 2005, "Hydrostatic gas journal bearings for micro-turbomachinery," *Journal of Vibration and Acoustics*, Transactions of the ASME, 127(2), pp. 157-164.

[8] G. Foshage and E. C. Lovelace, 2007 "An integrated magnetic/foil bearing and methods for supporting a shaft journal using the same," WO Patent WO/2007/011,366.

[9] H. Heshmat, H. Ming Chen, J. F. Walton II, January, 2000, "On the performance of Hybird Foil-Magnetic Bearings," *Journal of Engineering for Gas Turbines and Power*, 122, pp. 73-81.

[10] E. E. Swanson, H. Heshmat, April 2002, "Performance of a Hybrid Foil-Magnetic Bearing," *Journal of Engineering for Gas Turbines and Power*, 124, pp. 375-381.

[11] K. J. Eakman, T. L. Coons, M. Andres, and L. F. Miller, 1998, "Backup bearing for magnetic bearings," US Patents 5,714,818.

[12] H. Heshmat, 2005, "Hybrid Foil-magnetic Bearing with Improved Load Sharing," US Patent 6,965,181.

[13] Ye Tian, Yanhua Sun, Lie Yu, 2012, "Steady-State Control of Hybrid Foil-Magnetic Bbearings," *Proceedings of ASME Turbo Expo 2012*, June 11-15, 2012, Copenhagen, Denmark, GT2012-68394.

[14] Ye Tian, Yanhua Sun, Lie Yu, 2013, "Structural Stiffness and Damping Coefficients of a Multi-leaf Foil Bearing with Bump Foils Underneath," ASME J Eng Gas Turbines Power, 136(4), pp. 044501.

[15] Kasarda, M. E., Marshall, J., and Prins, R., 2007, "Active Magnetic Bearing Based Force Measurement Using the Multi-Point Technique," *Mechanics Research Communications*, 34(1), pp. 44-53.

[16] Ye Tian, Yanhua Sun, Lie Yu, 2010, "LQG Control of Hybrid Foil - Magnetic Bearing," *The twelfth international symposium on magnetic bearings*, Wuhan, China.